AGU PUBLICATIONS

Geophysical Research Letters

RESEARCH LETTER
10.1002/2016GL071402

Key Points:
- Three-dimensional displacements of a volcanic landslide created using pixel offset measurements between two synthetic aperture radar amplitude images
- Four meters of flank movement at Pacaya Volcano suggest serious instability hazard
- Episodic movement initiated by rapid triggers may promote volcano edifice instability without timely warning

Supporting Information:
- Supporting Information S1

Correspondence to:
L. N. Schaefer,
lnschaef@mtu.edu

Citation:
Schaefer, L. N., T. Wang, R. Escobar-Wolf, T. Oommen, Z. Lu, J. Kim, P. R. Lundgren, and G. P. Waite (2016), Three-dimensional displacements of a large volcano flank movement during the May 2010 eruptions at Pacaya Volcano, Guatemala, *Geophys. Res. Lett.*, *44*, doi:10.1002/2016GL071402.

Received 29 SEP 2016
Accepted 15 DEC 2016
Accepted article online 19 DEC 2016

Three-dimensional displacements of a large volcano flank movement during the May 2010 eruptions at Pacaya Volcano, Guatemala

L. N. Schaefer[1], T. Wang[2], R. Escobar-Wolf[1], T. Oommen[1], Z. Lu[2], J. Kim[2], P. R. Lundgren[3], and G. P. Waite[1]

[1]Department of Geological and Mining Engineering and Sciences, Michigan Technological University, Houghton, Michigan, USA, [2]Roy M. Huffington Department of Earth Sciences, Southern Methodist University, Dallas, Texas, USA, [3]Jet Propulsion Laboratory, California Institute of Technology, Pasadena, California, USA

Abstract Although massive flank failure is fairly common in the evolution of volcanoes, measurements of flank movement indicative of instability are rare. Here 3-D displacements from airborne radar amplitude images derived using an amplitude image pixel offset tracking technique show that the west and southwest flanks of Pacaya Volcano in Guatemala experienced large (~4 m), discrete landsliding that was ultimately aborted. Pixel offset tracking improved measurement recovery by nearly 50% over classic interferometric synthetic aperture radar techniques, providing unique measurements at the event. The 3-D displacement field shows that the flank moved coherently downslope along a complex failure surface involving both rotational and along-slope movement. Notably, the lack of continuous movement of the slide in the years leading up to the event emphasizes that active movement should not always be expected at volcanoes for which triggering factors (e.g., magmatic intrusions and eruptions) could precipitate sudden major flank instability.

1. Introduction

Massive flank failure is a fairly common process in the evolution of volcanoes, having occurred at over 400 volcanoes worldwide [*Siebert et al.*, 2006]. The resulting debris avalanche from a large volcanic slope failure can be extremely hazardous due to their size and mobility, resulting in 20,000 casualties in the past 400 years [*Siebert*, 1984]. However, few measurements of large, discrete flank movements exist at volcanoes, with most measured cases of unstable flanks exhibiting slow ($<$10 cm/yr) creep over years to decades [see *Ebmeier et al.*, 2010, and references therein]. The largest flank movement detected by space geodesy was captured by interferometric synthetic aperture radar (InSAR) ground deformation measurements at Pacaya Volcano in Guatemala, revealing ~3 m of displacement of the west and southwest flanks during explosive eruptions on 27 and 28 May 2010 [*Schaefer et al.*, 2015]. This movement was determined to be coeruptive, occurring sometime over the 2 day eruption that produced 1.3×10^7 m^3 of tephra and $1.6–6.4 \times 10^6$ m^3 of lava, categorizing the eruptions as a VEI 2–3 on the Volcano Explosivity Index (VEI). A NNW oriented trough developed concurrently with the eruptions and slope movement, measuring 50–80 m deep, 100 m wide, and extending 600 m from the summit (Figure 1). The development of this feature is likely due either to a NNW oriented magma intrusion and/or the flank movement itself. Given the magnitude of displacement and the history of flank collapse, with an ancestral collapse occurring 600–1500 years [*Kitamura and Matías*, 1995], this movement was considered to be an indication of severe edifice instability.

While InSAR captures the spatial extent of the coeruptive slope movement, phase jumps and a high deformation gradient prevent phase unwrapping [*Schaefer et al.*, 2015] and thus the retrieval of a continuous deformation field. Additionally, interferograms of this event suffer from phase decorrelation on the upper flanks due to changes in surface reflection characteristics and presumably large motions. Consequently, it is not possible to resolve the three-dimensional (3-D) surface displacement field using InSAR. Here a pixel offset tracking technique was applied to two tracks of UAVSAR (L-band, wavelength = 23.8 cm) images (one flying from S68°E to N68°W and one flying from N68°W to S68°E) acquired on 11 February 2010 and 26 April 2011 that span the 27 and 28 May 2010 eruptions. The 3-D displacement field was then estimated from the azimuth- and range-offset measurements.

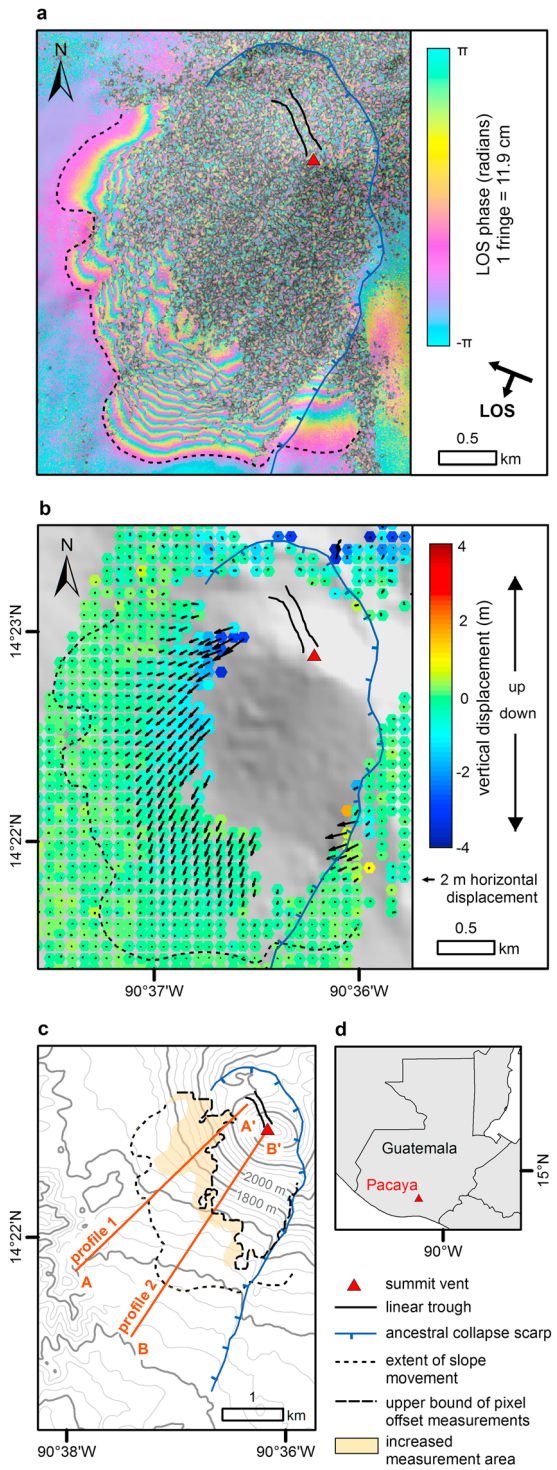

Figure 1. Location of Pacaya Volcano and results of 3-D displacement measurements. (a) UAVSAR interferogram of the slope movement, spanning 11 February 2010 to 26 April 2011. (b) Three-dimensional motion component results of SAR amplitude pixel offset measurements draped over the SRTM 1 arc digital elevation model. Horizontal components are indicated by arrows, with the arrow length corresponding to the displacement magnitude, and vertical components by colored points, with hotter colors indicating uplift and cooler colors indicating subsidence. The distal extent of slope movement is outlined from UAVSAR images in *Schaefer et al.* [2015]. The area to the southeast of the summit with vertical inflation and WSW horizontal movement corresponds to vent openings that produced a large lava flow during the eruptive event [see *Schaefer et al.*, 2015]. (c) Upper bound of offset measurements is shown to emphasize pixel tracking improvement of retrievable measurements, outlined in beige. (d) Location of Pacaya Volcano in Guatemala.

2. Methods

2.1. SAR Offset Measurements on Predetected Targets

Pixel offset measurements between two synthetic aperture radar (SAR) amplitude images can provide unambiguous ground displacement measurements in both the line of sight (LOS) direction and parallel to the along-track satellite flying direction [*Michel et al*., 1999]. Although pixel offset measurements are typically less accurate than slant range phase, being on the order of one tenth the accuracy of the pixel resolution (~2 m for UAVSAR), they allow for the full 3-D displacement field to be derived when both ascending and descending orbits are combined [e.g., *Fialko et al*., 2001]. In addition to conventional SAR image offset tracking methods, which cross correlates regularly spaced windows (e.g., 64×64 pixels) throughout an image, here strong reflectors were used to identify and focus the offset estimates if present. This target detection strategy can retrieve useful displacement information even when the corresponding interferogram appears completely decorrelated [e.g., *Wang and Jonsson*, 2015; *Wang et al*., 2015].

Two pairs of coregistered UAVSAR SAR images acquired on 11 February 2010 and 26 April 2011 were provided by the Jet Propulsion Laboratory. Cross-correlation windows with steps of half of the window size were distributed throughout the amplitude images to detect strong reflectors and increase measurement density. Next, both the azimuth and range offsets were estimated by cross correlating 64×64 pixel windows centered on the assigned locations (see supporting information for range and azimuth offsets). The topography-related offsets are expected to be negligible due to the small perpendicular baseline between UAVSAR acquisitions. Obvious outliers were removed from the results using 0.2 as a cross-correlation threshold.

2.2. Three-Dimensional Slope Displacements

The 3-D displacement field was created using a system of linear equations linking the azimuth- and range-offset measurements (d_{az} and d_{los}) to 3-D surface displacements U as follows [*Fialko et al*., 2001]:

$$\begin{bmatrix} -\sin\theta^a \cos\phi^a & \sin\theta^a \sin\phi^a & \cos\theta^a \\ -\sin\theta^d \cos\phi^d & \sin\theta^d \sin\phi^d & \cos\theta^d \\ \sin\phi^a & \cos\phi^a & 0 \\ \sin\phi^d & \cos\phi^d & 0 \end{bmatrix} \begin{bmatrix} U_e \\ U_n \\ U_u \end{bmatrix} = \begin{bmatrix} d^a_{los} \\ d^d_{los} \\ d^a_{az} \\ d^d_{az} \end{bmatrix} \quad (1)$$

where θ is the radar incidence angle, ϕ is the airplane heading angle, and superscripts a and d correspond to the ascending and descending flights, respectively. Using this system of equations, 3-D displacements were computed where at least three measurements existed within 100 m × 100 m windows uniformly distributed across the imaged area. Within the window, the variance of offsets from each direction was calculated and removed if larger than 0.3 m. Uncertainty was calculated based on the standard deviation of a window far from the volcano, assumed to be an area of no deformation. Given the full 3-D displacements, movement can then be decomposed into the vertical and along-profile horizontal directions using known aspect angles of the topographic profiles.

2.3. Persistent Scatterer Interferometric Synthetic Aperture Radar

To investigate evidence of movement prior to the coeruptive landslide, 19 InSAR pairs with high spatiotemporal coherence between 6 August 2007 and 29 March 2010 were used to calculate the LOS direction deformation rate using persistent scatterer InSAR (persistent scatterer interferometric, PSI) [*Ferretti et al*., 2001, 2011]. To maximize the density of PS points on the surface, both PSI and Small Baseline Subset techniques [*Berardino et al*., 2002] were applied using the StaMPS software package. A more detailed discussion of the methodology can be found in the supporting information [*Hooper*, 2008; *Ebmeier et al*., 2012; *Matías Gómez et al*., 2012; *Salzer et al*., 2014].

3. Results

Pixel offset measurements confirm high-magnitude landsliding movement of the SW flank originally revealed using InSAR [*Schaefer et al*., 2015]. The greatest amount of recoverable displacement occurred at higher elevations (maximum westward movement of 3.92 ± 0.02 m, southward movement of 2.90 ± 0.04 m, and downward movement of 2.95 ± 0.05 m), decreasing in magnitude to the toe of the slide (Figure 1a). Amplitude pixel offset tracking increased measurement recovery by 48%, or an area increase

of ~1.29 km^2, over classic InSAR techniques (Figure 1b), confirming that parts of the upper edifice were involved in the slope movement. Although pixel offset tracking cannot recover deformation on the upper southwest flanks due to severe surface disturbances, based on the smooth deformation field and the spatial extent of settlement posteruption [*Schaefer et al*., 2016], we speculate that displacements increase toward the summit, similar to the western flank. This is supported by significant deformation (~20 cm) of the ancestral collapse scarp located to the NNW of the linear trough measured with GPS in January of 2009 and 2011. The magnitude and direction of movement on the lower flanks is additionally supported by GPS measurements [*Zumberge et al*., 1997; *Hetland*, 2014] (see supporting information for more details). Given that the edifice is highly asymmetric, being built within the avalanche scarp of an ancestral volcano, the unstable area accounts for much of the current cone. Measurements to the NE of the ancestral collapse scarp show varying degrees of vertical displacement and a random distribution of horizontal components. These points are located in a highly vegetated area that experienced several tens of centimeters of tephra fall during the eruption, creating drastic surface changes. Thus, we consider these measurements to be unreliable. This is again confirmed by the GPS measurements, which show negligible movement in the area to the northeast of the ancestral collapse scarp.

The comprehensive spatial sampling of the pixel tracking measurements shows a smooth deformation field that spans the west and southwest flanks, with different gradients corresponding to different styles of movement. Profiles of 3-D displacement show these detailed landslide mechanics, with a notable decrease in vertical components of the slide at the boundary between the steep (~33°) upper cone above 1600 m above sea level and the shallower (~10°) lower flanks. On the west flank, which contains the most proximal measured points to the summit, the slope moved at an angle of ~30° below the horizontal at the highest elevations, shallowing to ~15° at the base of the slide (Figure 2a). This change in movement direction indicates rotation of the 1.5 km sliding mass. Instead of a thrust geometry downslope, which would resemble a classic rotational failure, the movement diminishes to slope parallel. On the southwest flank, which contains the most distal measured points, measurements recovered on the lower, shallow portion of the flank show that movement was nearly slope parallel at 11° below horizontal (Figure 2b). At the toe of the slide the movement direction steepens slightly, although the vertical components remain small (~30 cm or less). On both flanks, the profiles show shortening of the slope by a few meters over areas of 1–1.5 km. This shortening is likely too diffuse to cause significant bulging at the toe of the slide, a common feature seen at volcanoes with gravitationally driven slope movement [i.e., *van Wyk de Vries and Francis*, 1997].

The PSI analysis shows no continuous or episodic movement of the lower flanks in the years (August 2007 to March 2010) leading up to the 2010 eruption that would indicate long-term instability of the extent of material that moved (Figure 3; see supporting information for details). It is important to note that both the SAR acquisitions and GPS collection dates, on the order of months to years, prevent the retrieval of deformation in the weeks, days, and hours leading up to the flank movement. Thus, the possibility of very short term deformation prior to the eruptions cannot be ruled out.

4. Discussion

The most extreme case of documented flank deformation occurred at Mount St. Helens in 1980, when bulging of the northern flank on the order of 150 m over several months provided dramatic indication of magmatic intrusion into the volcano prior to catastrophic collapse [*Lipman and Mullineaux*, 1981]. Unlike Mount St. Helens, the low frequency of observations at Pacaya prevents us from determining the exact role of magma intrusion and eruption in the flank movement. Prior to the May 2010 eruptions, activity increased markedly in the weeks before the eruptions, with an increase in lava flows suggesting an increase in intrusion rate into the cone (*CONRED* bulletin reports, http://www.conred.gob.gt/). The formation of the NNW trending trough during the eruptions is the most obvious link between magma intrusion and slope movement, with an eruption from the lower end of the structure providing clear evidence that magma propagated through the feature. Substantial horizontal movement of the SW flank perpendicular to the trough also likely played a role in its formation, although the lack of measurements near the summit prevents us from directly correlating a landslide head scarp to the trough location. However, cracking along this NNW trend and the eruption of a large lava flow on the SE flank shortly after the explosive eruptions indicate that a tensional zone spans the entire cone [*Schaefer et al*., 2016]. The orientation of the magma intrusion and trough formation is

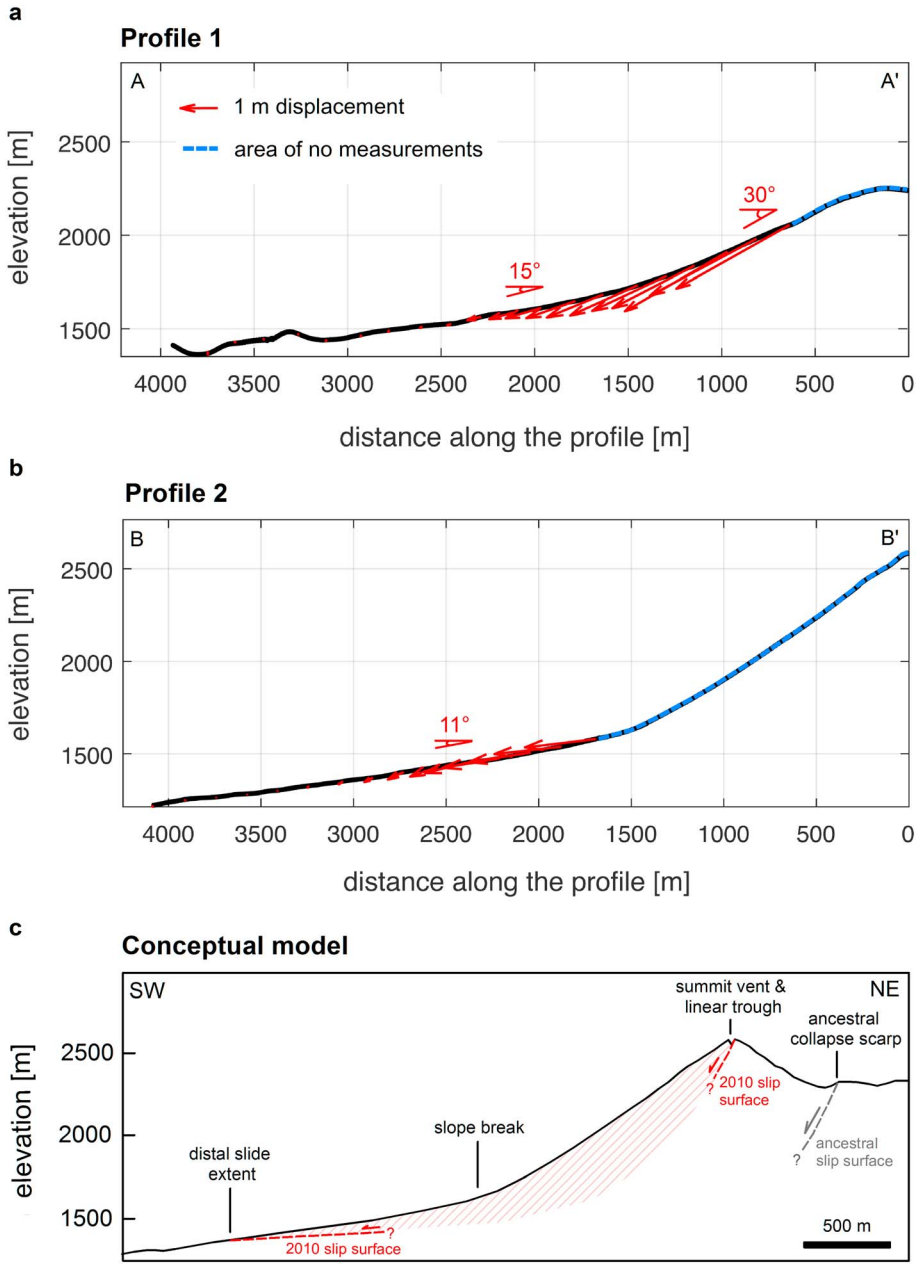

Figure 2. Cross sections of the slide and conceptual model of instability. (a and b) The total magnitude and angle of motion shown as vectors on different transects originating at Pacaya's summit, so that arrow length is proportional to displacement magnitude. Locations of the profiles are shown in Figure 1b. (c) Conceptual model of ancestral and 2010 sliding surfaces, with the cross section being an extension of Profile 2 in Figure 2b. The 2010 trough feature and angle of surface movement at the lowest elevation is extended inward, represented by red dashed lines, and the potential zone of unstable material is represented by the pink dashes. Currently, the head scarp of the landslide is drawn to coincide with the NNW trending linear trough feature. A lack of measurements near the summit prevents a clear recognition of the head scarp, which may be located farther to the NE, thus incorporating a greater volume of the edifice.

likely controlled by the local transtensional (ENE-WSW σ_3 component) stress regime [*Schaefer et al.*, 2013]. While models of a NNW striking dike intrusion can account for some of the measured deformation [*Okada*, 1985] (see supporting information for synthetic interferograms), large misfits arise due to a lack of measured deformation on the southeast and northwest flanks. Additionally, dike opening, even at shallow depths, produces deformation that covers a much larger area than that of the observed motions over the lower southwest flank. Thus, we conclude that much of the measured deformation is due to landslide propagation after triggering, preventing a direct correlation between the amount of dike opening and measured flank movement.

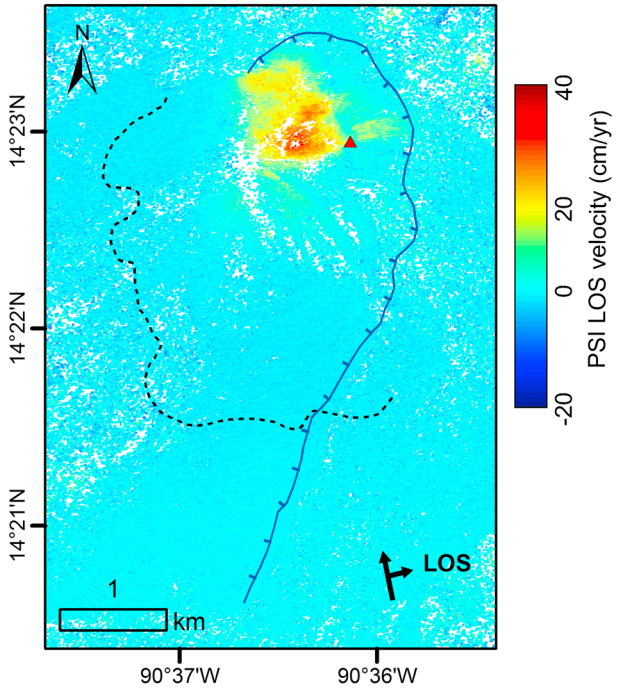

Figure 3. Mean line-of-sight (LOS) velocity map from permanent scatter InSAR analysis of ALOS interferograms spanning 6 August 2007 to 29 March 2010 shows no deformation of the lower flanks. Positive LOS change corresponds to surface movement away from the satellite, with black arrows representing the satellite heading and radar look directions.

The absence of long-term deformation prior to (PSI results Figure 3) and after [*Schaefer et al*., 2016] the slope movement suggests that the landslide was both rapidly triggered and arrested, likely contained to the explosive phases during the 2 day eruption. Magma-induced flank displacement on the order of tens of centimeters has been observed at smaller scales at other volcanoes such as Kilauea [*Swanson et al*., 1976], Piton de la Fournaise [*Sigmundsson et al*., 1999], and Etna [*Acocella et al*., 2003]. In these cases, the intrusions seem to temporally increase preexisting gravitational instabilities [*Delaney et al*., 1998; *Lundgren et al*., 2004; *Clarke et al*., 2013], even reactivating repeatedly (i.e., Kilauea Volcano) [*Swanson et al*., 1976; *Delaney and Denlinger*, 1999]. In nonvolcanic environments, large episodic movement surrounded by essentially static periods such as that seen at Pacaya can recur repeatedly [e.g., *Petley et al*., 2005; *Massey et al*., 2013; *Tiranti et al*., 2013; *Ronchetti et al*., 2010]. These reactivations tend to be correlated with specific triggers, often related to hydrologic variations such as rainfall or seasonal snowmelt. Studies of the now inactive San Andres Fault system on El Hierro (Canary Islands) indicate that a similar process on a larger scale occurred between 546 and 176 ka, in which a giant landslide appears to have aborted during the early stages of sliding [*Day et al*., 1997]. This was attributed primarily to the absence of pore fluid saturated rocks, which is a key factor controlling the initiation of debris avalanches in theoretical models [e.g., *Elsworth and Voight*, 1995]. Although there are no indications that Pacaya's edifice is saturated, intrusions into the edifice during the 2010 eruptions may have acted to temporally increase fluid pressures, triggering instability. While it is unclear what conditions must be met to promote failure, the magnitude of movement measured here and evidence of large movements at other volcanoes suggests that volcanic flanks are capable of experiencing significant displacements without the sliding mass propagating into a catastrophic debris avalanche.

Given the lack of measurements on the upper southwest flank and around the summit area, the full components of the landslide geometry cannot be revealed. However, the spatial extent of the material involved in the slide, extending nearly 3000 m from the summit vent and incorporating areas far beyond the steeper slopes, suggests a deep slip surface. Landslide volume (V) is commonly estimated from landslide area (A) in the form of $V = \alpha A^{\gamma}$, with scaling exponent (γ) and intercept (α) derived from field measurements [*Larsen et al*., 2010]. Using parameter estimates given by *Larsen et al*. [2010] for bedrock landslides ($\gamma = 1.35 \pm 0.01$ and $\log_{10}(\alpha) = -0.73 \pm 0.06$), and considering an area of 7 km^2 extending from the summit to the toe of the slope movement, the volume and average depth would be 0.32 km^3 and 46 m, respectively. However,

given that the dispersion for these exponential relationships is an order of magnitude (see plots in *Larsen et al*. [2010]), these values should be considered rough approximations. The possibility of surfaces at multiple depths (e.g., Las Isletas) [*van Wyk de Vries and Francis*, 1997] or multiple failure blocks (e.g., Mount St. Helens) [*Lipman and Mullineaux*, 1981] can also not be ruled out. Additionally, given the inherent structural complexities in a volcanic edifice, the slip surface is likely to be noncircular, such as the collapse scarps of other large volcanic sector collapses [*Siebert*, 1984]. Noncircular slip surfaces modeled in *Schaefer et al*. [2013] that include areas beyond the steeper slopes of the edifice such as that measured here suggest that the depth to the surface may be on the order of several hundreds of meters near the head scarp. If this is the case, the unstable mass may be similar to the volume that failed in the ancestral collapse event, estimated between 0.65 and $>1\ km^3$ of material [*Siebert et al*., 2006].

5. Conclusions

Unlike the continuous movement often measured on unstable volcano flanks, evidence from persistent scatterer InSAR at Pacaya Volcano suggests that large flank movements or catastrophic collapse may not be detectable long before they occur. Instead, episodic movements initiated by magmatic intrusions or other rapid triggers may promote edifice instability. Without high-frequency geodetic monitoring during eruptive episodes, short-term indications of impending large movement may be missed, preventing timely warning. Although remote sensing techniques such as InSAR are capable of creating high-density spatial maps of volcanic deformation, large movements can lead to decorrelation or unwrapping errors, prohibiting the extraction of useful measurements. Amplitude image pixel offset measurements applied to UAVSAR SAR images have proven capable of retrieving signal from decorrelated areas in SAR interferograms, allowing a 3-D displacement field to be estimated from the azimuth- and range-offset measurements. The resulting measurements provide insight into a unique landslide event at an active volcano with the potential to collapse catastrophically. The possibility of reactivation of the unstable mass should be considered a future hazard, particularly during magmatic intrusions or eruptive episodes.

Acknowledgments

L.S. acknowledges support provided by the NASA Earth and Space Science Fellowships Program (NNX13AO50H). T.W., J.W.K., and Z.L. acknowledge support from the NASA Earth Surface and Interior Program (NNX14AQ95G) and the Shuler-Foscue Endowment at Southern Methodist University. Raw UAVSAR (Uninhibited Aerial Vehicle Synthetic Aperture Radar) data were provided by the NASA Jet Propulsion Laboratory-California Institute of Technology. We thank Yang Zhang for her assistance in providing SLC images. PALSAR data from the ALOS-1 satellite mission operated by the Japanese Aerospace Exploration Agency (JAXA) were used under the terms and conditions of the Western North America Interferometric Synthetic Aperture Radar Consortium (WInSAR). DInSAR was processed using Gamma. PSI was processed using StaMPS. MATLAB functions to detect point-like targets in SAR images are available upon request. We thank Francisco Delgado and an anonymous reviewer for their help in improving this manuscript.

References

Acocella, V., B. Behncke, M. Neri, and S. D'Amico (2003), Link between major flank slip and 2002–2003 eruption at Mt. Etna (Italy), *Geophys. Res. Lett.*, *30*, doi:10.1029/2003GL018642.

Berardino, P., G. Fornaro, R. Lanari, and E. Sansosti (2002), A new algorithm for surface deformation monitoring based on Small Baseline Differential SAR interferograms, *IEEE Trans. Geosci. Remote Sens.*, *40*, 2375–2383, doi:10.1109/TGRS.2002.803792.

Clarke, D., F. Brenguier, J. L. Froger, N. M. Shapiro, A. Peltier, and T. Staudacher (2013), Timing of a large volcanic flank movement at Piton de la Fournaise Volcano using noise-based seismic monitoring and ground deformation measurements, *Geophys. J. Int.*, *276*, doi:10.1093/gji/ggt276.

Day, S. J., J. C. Carracedo, and H. Guillou (1997), Age and geometry of an aborted rift flank collapse: The San Andres fault system, El Hierro, Canary Islands, *Geol. Mag.*, *4*, 523–537.

Delaney, P. T., and R. P. Denlinger (1999), Stabilization of volcanic flanks by dike intrusion: An example from Kilauea, *Bull. Volcanol.*, *61*, 356–362, doi:10.1007/s004450050278.

Delaney, P. T., R. P. Denlinger, M. Lisowski, A. Miklius, P. G. Okubo, A. T. Okamura, and M. K. Sako (1998), Volcanic spreading at Kilauea, 1976–1996, *J. Geophys. Res.*, *103*, 18,003–18,023, doi:10.1029/98JB01665.

Ebmeier, S., J. Biggs, T. Mather, G. Wadge, and F. Amelung (2010), Steady downslope movement on the western flank of Arenal volcano, Costa Rica, *Geochem. Geophys. Geosyst.*, *11*, Q12004, doi:10.1029/2010GC003263.

Ebmeier, S. K., J. Biggs, T. A. Mather, J. R. Elliott, G. Wadge, and F. Amelung (2012), Measuring large topographic change with InSAR: Lava thicknesses, extrusion rate and subsidence rate at Santiaguito volcano, Guatemala, *Earth Planet. Sci. Lett.*, *335*, doi:10.1016/j.epsl.2012.04.027.

Elsworth, D., and B. Voight (1995), Dike intrusion as a trigger for large earthquakes and the failure of volcano flanks, *J. Geophys. Res.*, *100*, 6005–6024, doi:10.1029/94JB02884.

Ferretti, A., C. Prati, and F. Rocca (2001), Permanent scatterers in SAR interferometry, *IEEE Trans. Geosci. Remote Sens.*, *39*, 8–20, doi:10.1109/36.898661.

Ferretti, A., A. Fumagalli, F. Novali, C. Prati, F. Rocca, and A. Rucci (2011), A new algorithm for processing interferometric data-stacks: SqueeSAR, *IEEE Trans. Geosci. Remote Sens.*, *49*, 3460–3470, doi:10.1109/TGRS.2011.2124465.

Fialko, Y., M. Simons, and D. Agnew (2001), The complete (3-D) surface displacement field in the epicentral area of the 1999 M_W7.1 Hector Mine Earthquake, California, from space geodetic observations, *Geophys. Res. Lett.*, *28*, 3063–3066, doi:10.1029/2001GL013174.

Hetland, B. R. (2014), A surface displacement analysis for Volcan Pacaya from October 2001 through March 2013 by means of 3-D modeling of precise position GPS data, MS Thesis, Michigan Technological Univ., 84 p.

Hooper, A. (2008), A multi-temporal InSAR method incorporating both persistent scatterer and small baseline approaches, *Geophys. Res. Lett.*, *35*, L16302, doi:10.1029/2008GL034654.

Kitamura, S., and O. Matías (1995), *Tephra Stratigraphic Approach to the Eruptive History of Pacaya Volcano, Guatemala: Science Reports, Seventh Ser., Geogr.*, vol. 45, pp. 1–41, Tohoku Univ., Sheffield, England.

Larsen, I. J., D. R. Montgomery, and O. Korup (2010), Landslide erosion controlled by hillslope material, *Nat. Geosci.*, *3*(4), 247–251, doi:10.1038/ngeo776.

Lipman, P. W., and D. R. Mullineaux (Eds.) (1981), The 1980 eruptions of Mount St. Helens, Washington (No. 1250), US Dept. of the Interior, US Geol. Surv.

Lundgren, P., F. Casu, M. Manzo, A. Pepe, P. Berardino, E. Sansosti, and R. Lanari (2004), Gravity and magma induced spreading of Mount Etna volcano revealed by satellite radar interferometry, *Geophys. Res. Lett*, *31*, L04602, doi:10.1029/2003GL018736.

Massey, C. I., D. N. Petley, and M. J. McSaveney (2013), Patterns of movement in reactivated landslides, *Eng. Geol.*, *159*, 1–19, doi:10.1016/j.enggeo.2013.03.011.

Matías Gómez, R. O., W. I. Rose, J. L. Palma, and R. Escobar-Wolf (2012), *Notes on a Map of the 1961–2010 Eruptions of Volcán de Pacaya, Guatemala*, *Geol. Soc. Am. Digital Map Chart Ser.*, vol. 10, doi:10.1130/2012.DMCH010.

Michel, R., J. P. Avouac, and J. Taboury (1999), Measuring ground displacements from SAR amplitude images: Application to the Landers earthquake, *Geophys. Res. Lett.*, *26*, 875–878, doi:10.1029/1999GL900138.

Okada, Y. (1985), Surface deformation due to shear and tensile faults in a half-space, *Bull. Seismol. Soc. Am.*, *75*, 1135–1154.

Petley, D. N., F. Mantovani, M. H. Bulmer, and A. Zannoni (2005), The use of surface monitoring data for the interpretation of landslide movement patterns, *Geomorphology*, *66*, 133–147, doi:10.1016/j.geomorph.2004.09.011.

Ronchetti, F., L. Borgatti, F. Cervi, and A. Corsini (2010), Hydro-mechanical features of landslide reactivation in weak clayey rock masses, *Bull. Eng. Geol. Environ.*, *69*(2), 267–274, doi:10.1007/s10064-009-0249-3.

Salzer, J. T., M. Nikkhoo, T. R. Walter, H. Sudhaus, G. Reyes-Dávila, M. Bretón, and R. Arámbula (2014), Satellite radar data reveal short-term pre-explosive displacements and a complex conduit system at Volcán de Colima, Mexico, *Front. Earth Sci.*, *2*, doi:10.3389/feart.2014.00012.

Schaefer, L., Z. Lu, and T. Oommen (2015), Dramatic volcanic instability revealed by InSAR, *Geology*, *43*, 743–746, doi:10.1130/G36678.1.

Schaefer, L. N., T. Oommen, C. Corazzato, A. Tibaldi, R. Escobar-Wolf, and W. I. Rose (2013), An integrated field-numerical approach to assess slope stability hazards at volcanoes: The examples of Pacaya Volcano, Guatemala, *Bull. Volcanol.*, *75*, 1–18, doi:10.1007/s00445-013-0720-7.

Schaefer, L. N., Z. Lu, and T. Oommen (2016), Post-eruption deformation processes measured using ALOS-1 and UAVSAR InSAR at Pacaya Volcano, Guatemala, *Remote Sens.*, *8*, doi:10.3390/rs8010073.

Siebert, L. (1984), Large volcanic debris avalanches: Characteristics of source areas, deposits, and associated eruptions, *J. Volcanol. Geothermal Res.*, *22*, 163–197, doi:10.1016/0377-0273(84)90002-7.

Siebert, L., G. E. Alvarado, J. W. Vallance, and B. van Wyk De Vries (2006), Large-volume volcanic edifice failures in Central America and associated hazards, *Geol. Soc. Am. Spec. Pap.*, *412*, 1–26, doi:10.1130/2006.2412(01).

Sigmundsson, F., P. Durand, and D. Massonnet (1999), Opening of an eruptive fissure and seaward displacement at Piton de la Fournaise volcano measured by RADARSAT satellite radar interferometry, *Geophys. Res. Lett.*, *2*, 533–536, doi:10.1029/1999GL900055.

Swanson, D. A., W. A. Duffield, and W. S. Fiske (1976), Displacement of the south flank of Kilauea Volcano: The result of foreceful intrusion of magma into the rift zones, *Geol. Surv. Prof. Pap.*, *963*, 1–39.

Tiranti, D., D. Rabuffetti, A. Salandin, and M. Tararbra (2013), Development of a new translational and rotational slides prediction model in Langhe hills (north-western Italy) and its application to the 2011 March landslide event, *Landslides*, *10*(2), 121–138, doi:10.1007/s10346-012-0319-7.

Van Wyk de Vries, B., and P. W. Francis (1997), Catastrophic collapse at stratovolcanoes induced by gradual volcano spreading, *Nature*, *387*, 387–390, doi:10.1038/387387a0.

Wang, T., and S. Jonsson (2015), Improved SAR amplitude image offset measurements for deriving three-dimensional coseismic displacements, *IEEE J. Sel. Top. Appl. Earth Obs. Remote Sens.*, *8*, 3271–3278, doi:10.1109/JSTARS.2014.2387865.

Wang, T., M. P. Poland, and Z. Lu (2015), Dome growth at Mount Cleveland, Aleutian Arc, quantified by time series TerraSAR-X imagery, *Geophys. Res. Lett.*, *42*, 10,614–10,621, doi:10.1002/2015GL066784.

Zumberge, J. F., M. B. Heflin, D. C. Jefferson, M. M. Watkins, and F. H. Webb (1997), Precise point positioning for the efficient and robust analysis of GPS data from large networks, *J. Geophys. Res.*, *102*, 5005–5017, doi:10.1029/96JB03860.